International Journal of Concrete Structures and Materials

RESEARCH

Open Access

Dynamic Compressive Performance of Recycled Concrete Considering the Effects of Pretreatment of Recycled Coarse Aggregate and Calcium Leaching

Jian-Hua Jiang[1*], Fu-Liang Ma[1], Si-An Chen[1], Wei Zhang[1] and Si-Qi Zhao[1]

Abstract

To promote the resource utilization of construction solid waste and realize the sustainable development of building materials, it is an effective way to develop the recycled aggregate concrete. This study first examined the pretreatment effect of 5% water glass solution on recycled coarse aggregates (RCAs) by soaking them for varying durations. Then, the dynamic compressive performance tests were conducted on the pretreated recycled coarse aggregate concrete (PRCAC) using the split Hopkinson pressure bar device, considering the effects of the soaking duration of RCAs, the incorporation ratio of pretreated RCAs (PRCAs), and the calcium leaching. The results indicate that the water glass treatment improves the pore structure of RCA, reducing its water absorption, crushing index, and porosity. After 12 h of soaking in the water glass solution, the water absorption, crushing index, and porosity of RCA decreased by 13.7%, 11.3%, and 11.2%, respectively. Dynamic compressive strength and dynamic increase factor (DIF) of PRCAC are sensitive to strain rate, and increase with the increase of the strain rate. The dynamic compressive strength of PRCAC exhibits a positive correlation with the incorporation ratio of PRCAs and a negative correlation with the duration of calcium leaching. Additionally, the sensitivity of PRCAC to strain rate is negatively correlated with the incorporation ratio of PRCA and positively correlated with leaching duration. As the soaking duration of RCAs increases, the dynamic compressive strength of PRCAC first increases and then decreases. The degree of strength degradation of PRCAC due to calcium leaching decreases as the soaking duration of RCAs increases. The above research findings contribute to the improvement of the performance of recycled concrete and the correct evaluation of its dynamic mechanical properties.

Keywords Recycled aggregate concrete, Pretreatment of RCAs, Water glass, Calcium leaching, Dynamic compressive performance, Strain rate

1 Introduction

In recent years, with the rapid development of the social economy, the challenge of handling construction waste has become increasingly severe. Over the past decade, approximately 2.4 billion tons of construction waste have been generated annually in China, which is 15 times that of urban solid waste (Duan et al., 2019). A large volume of construction waste not only occupies the valuable land space, increases construction costs, and hinders economic development, but also causes environmental

Journal information: ISSN 1976-0485 / eISSN 2234-1315.

*Correspondence:
Jian-Hua Jiang
jjhzxh@hhu.edu.cn
[1] College of Civil and Transportation Engineering, Hohai University, Nanjing 210024, People's Republic of China

pollution and poses threats to public health (Bao, 2023; Bao et al., 2023; Tafesse et al., 2022). Recycling construction waste is currently the most effective method to handle this issue (Ding et al., 2023; Li et al., 2023; Wang et al., 2024). The utilization of construction waste as recycled aggregates for producing recycled aggregate concrete (RAC) conserves natural resources while mitigating environmental pollution (Tan et al., 2025; Xing et al., 2023). However, the high porosity and weak interface transition zone caused by the old mortar attached to recycled coarse aggregate (RCA) severely restrict the application of RAC in the main structure (Lu et al., 2024; Verian et al., 2018; Zhang et al., 2025). Especially under dynamic loads such as earthquakes and impacts, the mechanism of mechanical performance degradation of RAC is not yet clear, which has become a key scientific problem restricting its engineering applications.

Due to the adverse effects of low-quality recycled aggregates on the performance of concrete, various methods such as removing old mortar, polymer pretreatment, and nano-modification are commonly used to improve the performance of recycled aggregates and concrete in practical engineering. The removal of old mortar can be achieved through techniques such as ball milling, thermal treatment, and acidic dissolution, which enhance the performance of recycled aggregates by eliminating residual cement paste from their surfaces (Dilbas et al., 2019; Khoury et al., 2018; Petrou, 2021; Wu et al., 2023). Spaeth and Djerbi Tegguer (Spaeth & Djerbi Tegguer, 2013) demonstrated that silicon-based polymer pretreatment of recycled aggregates significantly reduces water absorption and enhances fragmentation resistance. Nano materials such as nano-SiO_2 and nano-$CaCO_3$ can enhance the bonding strength between cement mortar and aggregates, thereby improving the mechanical properties of RAC (Rezaei et al., 2023; Zhang et al., 2015). In addition to nano-materials and polymer modification, water glass and microorganisms can also be used to pretreat recycled aggregates. Water glass can densify the microstructure of recycled aggregates, thereby improving the mechanical and durability properties of RAC (Luo et al., 2023; Yang et al., 2022; Yin et al., 2023; Zhang et al., 2021). Biological deposition treatment can enhance the uniformity of precipitates on the aggregate surface, further improving the strength and durability of recycled aggregates (Zhang et al., 2023a).

Current research primarily examines how pretreating recycled aggregates affects the static mechanical properties and durability of RAC. However, concrete structures often face dynamic loads like explosions, earthquakes, and impacts, making it essential to study dynamic performance of RAC. Unlike static loading, dynamic loading significantly alters concrete's mechanical response, with strain rate being a key factor. To study the dynamic mechanical properties of concrete at various strain rates, dynamic mechanical tests are typically conducted using electro-hydraulic servo testing machines, drop-weight impact testers, and split Hopkinson pressure bar (SHPB) devices (Han & Tian, 2018; Kong et al., 2020; Taghipoor & Sadeghian, 2022; Zhao et al., 2023). Guo et al. (2019) proposed a calculation method for the overall damage energy consumption of pretreated recycled aggregate concrete beams under impact. Xiong et al. (2021) evaluated the dynamic bond behavior of fiber-wrapped basalt fiber-reinforced polymer (BFRP) bars embedded in sea sand and recycled aggregate concrete using high-strain-rate pull-out tests. Selyutina and Smirnov (2023) investigated the effects of the incorporation ratio of recycled aggregate and fiber type on the fracture critical stress of concrete, and constructed the stress/strain rate dependencies of critical stress using incubation time. Wang and Xiao (2018) investigated the effects of strain rates, the stirrup confinement, and the incorporation ratio of recycled aggregate on the dynamic mechanical behaviors of confined RAC. Tang et al. (2020) found that the dynamic compressive performance of fly ash/slag-based geopolymeric recycled aggregate concrete exhibited strong strain rate sensitivity. Additionally, the incorporation of multi-walled carbon nanotubes and nano materials (silicon dioxide and calcium carbonate) improves the dynamic compressive performance of RAC (Allujami et al., 2022; Li et al., 2016).

Given the potential for concrete structures to be subjected to sulfate attack, acid attack, and calcium leaching, it is valuable to consider the effects of these attacks when studying the dynamic mechanical properties of concrete (Arjomandi et al., 2023). Calcium leaching of concrete is a key issue affecting the durability of hydraulic and underground structures. Its mechanism is driven by the concentration gradient between the environmental medium and cement hydration products. This gradient causes continuous dissolution and precipitation of calcium hydroxide, destabilizing the C–S–H gel. As a result, the concrete matrix experiences increased porosity, deterioration of mechanical properties, and even risks structural failure (An et al., 2025; Wu et al., 2019). Due to microstructural defects, recycled aggregate concrete is more susceptible to calcium leaching than conventional concrete. Jiang et al. (2022, 2024) demonstrated through accelerated dissolution tests using ammonium chloride solution that the resistance of RAC to calcium leaching decreases significantly with both increasing replacement ratios of RCAs and higher initial damage degrees of concrete. Wu et al. (2025) found that calcium leaching accelerates chloride penetration in RAC and that porosity

Table 1 Main chemical components of cement (%)

CaO	SiO_2	Al_2O_3	Fe_2O_3	TiO_2	MgO	SO_3	K_2O	Na_2O	LOI
62.60	21.35	4.67	3.31	0.28	3.08	2.25	0.54	0.21	1.71

Table 2 Technical specifications of coarse aggregates

Types	Particle size (mm)	Bulk density (kg/m^3)	Apparent density (kg/m^3)	Water absorption ratio (%)	Mud content (%)	Crushing index (%)
RCA	5–20	1327	2618	6.20	0.8	14.1
NCA	5–20	1435	2725	2.34	0.3	8.2

increases from the internal leached surface toward the exposed surface due to calcium leaching.

Previous research has shown that pre-treatment techniques, such as physical and chemical strengthening, can improve the performance of recycled concrete aggregates. However, there is still insufficient research on the differences in pre-treatment effects under dynamic load conditions. Meanwhile, in recent years, scholars have found that calcium leaching significantly reduces the mechanical properties of concrete under long-term environmental exposure, and RAC is more susceptible to such damage due to its porous nature. Currently, there is a lack of research on the combined effects of these two factors (pre-treatment and calcium leaching) on the dynamic performance of RAC. Therefore, this study first pretreated the recycled coarse aggregates (RCAs) with a water glass solution due to its economic and practical advantages. Then, dynamic compressive performance tests were conducted on concrete prepared by the pretreated RCAs (PRCAs) at various strain rates using a split Hopkinson pressure bar (SHPB) device. The effects of pretreatment duration, PRCA incorporation ratio, and calcium leaching were also investigated. This study not only contributes to improving the theoretical system of dynamic mechanics for recycled concrete, but also provides data support to enhance the engineering applications of recycled aggregates, thereby promoting the development of high-performance construction waste recycling technologies.

2 Experimental Schemes

2.1 Materials

The cementitious material used is Grade 42.5 ordinary Portland cement, in accordance with Chinese Standard GB 175-2020, and its chemical composition is shown in Table 1. Coarse aggregates include natural coarse aggregate (NCA) and recycled coarse aggregate (RCA) sourced from crushed waste concrete. The properties of these coarse aggregates are listed in Table 2. Fine aggregate is ordinary river sand with a fineness modulus of 2.5. The particle size distributions for both coarse and fine aggregates are shown in Fig. 1, which comply with the requirements of Chinese Standard GB/T 14685-2022. The experimental water is ordinary tap water.

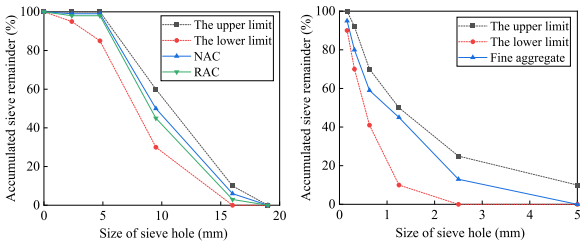

(a) Coarse aggregate (b) Fine aggregate

Fig. 1 Particle size distribution for the aggregates

2.2 Mixture Proportions of Concrete

Recycled aggregate concrete (RAC) was prepared by replacing RCAs with the pretreated RCAs (PRCAs) in this study. To explore a reasonable pretreatment scheme for RCAs, three pretreatment durations (i.e. soaking time t_s in water glass solution) were designed for the experiment, which were 1.5 h, 5.0 h, and 12.0 h, respectively. Meanwhile, three types of PRCA incorporation ratio (ρ_{prca}) were designed according to Chinese Standard JGJ/T443-2018, including 35%, 70%, and 100%. The water-cement ratio for the concrete was 0.40. The mixture proportions of concrete are listed in Table 3. The natural coarse aggregate concrete (NCAC) and ordinary recycled coarse aggregate concrete (RCAC) were control groups. Concretes prepared by partially or completely replacing RCAs with PRCAs were denoted as PRCAC. To account for the differences in water absorption among the different coarse aggregates, the different amounts of extra water were added during mixing to eliminate the influence of aggregates on the effective water-cement ratio.

Table 3 Mixture proportions of concrete with different incorporation ratios of PRCAs

Groups	ρ_{prca} (%)	t_s (h)	NCA (kg/m^3)	PRCA (kg/m^3)	RCA (kg/m^3)	Cement (kg/m^3)	Sand (kg/m^3)	Water (kg/m^3)	Extra water (kg/m^3)
NCAC	0	0	1165.0	0	0	450.0	655.0	180.0	27.3
RCAC	0	0	0	0	1165.0	450.0	655.0	180.0	72.2
A-PRCAC-1.5	35.0	1.5	0	407.8	757.3	450.0	655.0	180.0	71.0
A-PRCAC-5		5.0	0	407.8	757.3	450.0	655.0	180.0	69.0
A-PRCAC-12		12.0	0	407.8	757.3	450.0	655.0	180.0	68.8
B-PRCAC-1.5	70.0	1.5	0	815.5	349.5	450.0	655.0	180.0	69.8
B-PRCAC-5		5.0	0	815.5	349.5	450.0	655.0	180.0	65.7
B-PRCAC-12		12.0	0	815.5	349.5	450.0	655.0	180.0	65.3
C-PRCAC-1.5	100.0	1.5	0	1165.0	0	450.0	655.0	180.0	68.7
C-PRCAC-5		5.0	0	1165.0	0	450.0	655.0	180.0	62.9
C-PRCAC-12		12.0	0	1165.0	0	450.0	655.0	180.0	62.3

The amount of extra water was calculated based on the mass of the coarse aggregate in the unit volume of concrete multiplied by the water absorption of the aggregate.

2.3 Design and Preparation of Specimens

Dynamic mechanical performance tests on the concrete were conducted using cylindrical specimens with a length-to-diameter ratio of 1:2 (Liu et al., 2022). Cube specimens with a side length of 100 mm were prepared for static mechanical tests. The concrete mixture, produced using a drum mixer, was poured into plastic molds with dimensions of 100 mm × 100 mm × 100 mm for the cubes and cylindrical PVC pipes with an inner diameter of 70 mm and a height of 150 mm for the cylindrical specimens. The slump of all mixtures ranged between 55 and 60 mm, meeting the requirements of Chinese Standard GB/T 50164-2021. The concrete was vibrated and compacted using a vibration table. According to Chinese Standard GB/T 50081-2019, the specimens were demolded after 24 h and cured in a standard curing room (temperature of 20 ± 2 °C, relative humidity ≥ 95%) for 28 days. After curing, the uneven surfaces on both ends of the cylindrical specimens were cut off, and the specimens were then cut longitudinally into four cylindrical specimens, each with a diameter of 70 mm and a height of 35 mm, as shown in Fig. 2.

(a) Concrete pouring (b) Specimen cutting

Fig. 2 Schematic diagrams of cylindrical specimen preparation

2.4 Experimental Methods

2.4.1 Pretreatment of RCAs

The RCAs were pretreated by immersion in a water glass solution, with sodium silicate being the main component. Water glass precipitates silicate gel, which has strong adhesion. The silicate gel fills the pores and microcracks in the RCA and forms a stronger outer coating on its surface (Güneyisi et al., 2014). Additionally, sodium silicate reacts with hydration products such as calcium hydroxide in the old mortar adhered to the RCA, generating C–S–H gel, which further fills the pores and cracks, improving the performance of the RCA (Qiu et al., 2024). Water glass solution with a concentration of 5% was prepared by mixing water glass powder with water in a 1:19 mass ratio. The RCA samples were then immersed in the water glass solution, with the liquid level maintained at 5 mm above the samples throughout the soaking period. Refer to the relevant existing research and the pre-test, the soaking durations were designed to be 1.5 h, 5.0 h, and 12.0 h, respectively (Qiu et al., 2024). The day before concrete mixing, the pretreated RCAs were stored in a dry plastic container under normal indoor conditions.

2.4.2 Testing of Aggregate Performance

To evaluate the pretreatment effect of the water glass solution on RCAs, the basic physical properties, including apparent density (ρ_0), water absorption ratio (W_m), and crushing index (δ_a), were tested both before and after pretreatment, according to Chinese Standard GB/T 14685-2011.

2.4.3 Accelerated Calcium Leaching Test

To study the effect of calcium leaching on the dynamic mechanical properties of concrete, the ammonium chloride (NH_4Cl) solution was used to accelerate the calcium leaching in PRCAC with the ρ_{prca} of 100% (Zhang et al., 2023b). The main principle of accelerated calcium leaching is that NH_4Cl reacts with the hydration products, $Ca(OH)_2$ and C–S–H gel, inside the concrete to generate the soluble substance $CaCl_2$ (Jiang et al., 2022). The concentration of the NH_4Cl solution was 5 mol/L. The leaching durations were 14 days, 28 days, and 42 days, respectively.

2.4.4 Dynamic Compressive Performance Test

The dynamic compressive performance tests on cylindrical concrete specimens were performed using a split Hopkinson pressure bar (SHPB) device with a bar diameter of 74 mm. The apparatus mainly consists of an SHPB loading system and a data acquisition system. Air pressure was controlled using a point pressure gauge to achieve the desired value before releasing the bullet. To study the dynamic compressive performance of concrete under different strain rates, four air pressure values were applied, i.e., 0.40 MPa, 0.45 MPa, 0.50 MPa, and 0.55 MPa. The bullet exited the chamber and collided with the incident bar to generate an incident wave $\varepsilon_I(t)$. The incident wave passed through the shaper, the incident bar and the specimen sequentially, then continued to the transmission bar, generating a transmitted wave $\varepsilon_T(t)$. The remaining incident wave was reflected back to the incident bar at the connection between the specimen and the incident bar, creating a reflected wave $\varepsilon_R(t)$. Data was measured by strain gauges and transmitted to the strain instrument, which then sent the data to the analysis system. Based on the assumption of a one-dimensional stress wave and stress uniformity, the stress $\sigma_s(t)$, strain $\varepsilon_s(t)$, and strain rate $\dot{\varepsilon}_s(t)$ of the concrete specimen were obtained as follows:

$$\sigma_s(t) = E_b\left(\frac{A_b}{A_s}\right)\varepsilon_T(t) \tag{1}$$

$$\varepsilon_s(t) = -\frac{2C_0}{l}\int_0^t \varepsilon_R(t)dt \tag{2}$$

$$\dot{\varepsilon}_s(t) = -\frac{d\varepsilon_s(t)}{dt} \tag{3}$$

where E_b is the elastic modulus of the bar; A_b is the cross-sectional area of the bar; C_0 is the wave velocity; l is the axial length of the specimen; A_s is the cross-sectional area of the specimen.

2.4.5 Microscopic Structure Analysis

To explore the strengthening mechanism of water glass on RCA, low-field nuclear magnetic resonance (LF-NMR) technology was used to collect lateral relaxation time signals and characterize the pore structure and pore size distribution of the sample material (Wyrzykowski et al., 2017). After 24 h of vacuum saturation, the porosity and transverse relaxation signal T2 attenuation curve were measured using the CPMG sequence pre-set in the LF-NMR analyzer (Zhao et al., 2021). After inverting the T2 signal attenuation curve using the SIRT method, the distribution of the T2 signal quantity corresponding to the transverse relaxation time T2 was obtained and finally converted into the pore volume distribution for each pore size in the sample. In addition, the microstructure of the concrete was observed using a scanning electron microscope.

3 Effect of Water Glass Pretreatment on the Properties of RCAs

3.1 Apparent Density ρ_0

Fig. 3a shows the measured results for apparent density of RCAs after being soaked in the water glass solution for different durations (t_s). The ρ_0 of the pretreated RCAs is higher than that of the unpretreated ones, and increases gradually with the increase of t_s. The ρ_0 increased by 1.7%, 2.4% and 2.8% after soaked for 1.5 h, 5.0 h, and 12.0 h, respectively. This indicates that sodium silicate has a

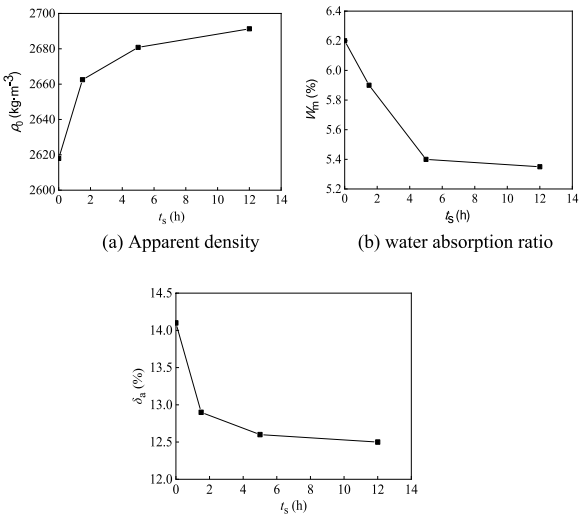

(a) Apparent density (b) water absorption ratio

(c) Crushing index

Fig. 3 Basic physical and mechanical performances of RCAs with different soaking durations in water glass solution

positive effect on filling the mortar cracks and pores on the surface of the aggregate, enhancing its compactness.

3.2 *Water Absorption Ratio W_m*

Change in the W_m of RCAs with different soaking durations (t_s) in water glass solution is shown in Fig. 3b. As the t_s increases, the W_m of RCAs gradually decreases. The W_m decreased by 4.8%, 12.9%, and 13.7% for t_s of 1.5 h, 5.0 h, and 12.0 h respectively, but it remained significantly higher than that of NCA. In addition, the decrease rate of the W_m gradually slows down with increasing t_s. As the t_s increased from 0 to 5.0 h, the decrease in the W_m was approximately linear, but beyond 5.0 h, further soaking had little additional effect, as the surface pores and cracks of the PRCA had become saturated.

3.3 *Crushing Index δ_a*

Change in the δ_a of RCAs with different soaking durations (t_s) in water glass solution is shown in Fig. 3b. The δ_a of RCAs soaked in water glass has a downward trend, and its reduction rate gradually decreases with the increase of t_s. Compared to the δ_a of unpretreated RCA, that of PRCAs with t_s of 1.5 h, 5.0 h, and 12.0 h decreased by 8.5%, 10.6%, and 11.3%, respectively. Although the δ_a of RCA soaked in water glass solution for 12.0 h was the smallest, it remained about 1.5 times that of NCA.

3.4 Porosity φ

The measurement results for the ϕ of RCAs before and after soaking in water glass solution are shown in Fig. 4. The water glass pretreatment can reduce the ϕ of recycled aggregates. After soaking for 1.5 h, 5.0 h, and 12.0 h, the ϕ of PRCAs decreased by 6.6%, 7.3%, and 11.2%, respectively. This is because the silicate gel precipitated from the hardening of water glass fills the internal pores of the RCA, and the water glass reacts with the calcium hydroxide in the old mortar of the RCA to form C–S–H, further filling internal voids and enhancing density (Qiu et al., 2024).

3.5 Pore Size Distribution

The pore size distributions of PRCAs with different soaking durations in water glass solution are shown in Fig. 5. After water glass pretreatment, both the peak value and peak area of the main peak in the pore size distribution of RCA decrease, with the most significant reduction occurring at a strengthening duration of 12.0 h. The pores of RCA can be categorized into four types based on size, namely gel pores, transitional pores, capillary pores, and macropores (Qiu et al., 2024). The relative pore volume proportions of these four types (compared to the total pore volume of RCA) are listed in Table 4. RCA1, RCA2, and RCA3 are three recycled coarse aggregate samples, while PRCA1-1.5, PRCA2-5.0, and PRCA3-12.0 refers to samples RCA1, RCA2, and RCA3 after water glass pretreatment for 1.5 h, 5.0 h, and 12.0 h, respectively. After pretreatment, the proportions of capillary pores and macropores decreased, whereas those of gel pores and transitional pores increased slightly. Specifically, the macropores in RCA decreased by 27.04%, 28.75%, and 34.55% corresponding to the soaking duration of 1.5 h, 5.0 h, and 12.0 h, respectively. However, no significant variation in the most probable pore radius of RCA was observed with increasing soaking duration in water glass solution.

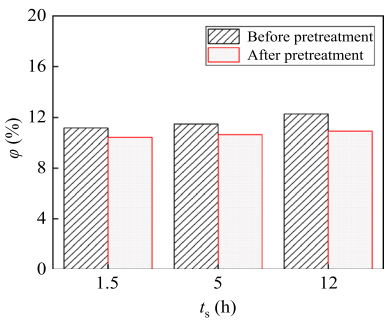

Fig. 4 Changes in porosity of RCAs with different soaking durations in water glass solution

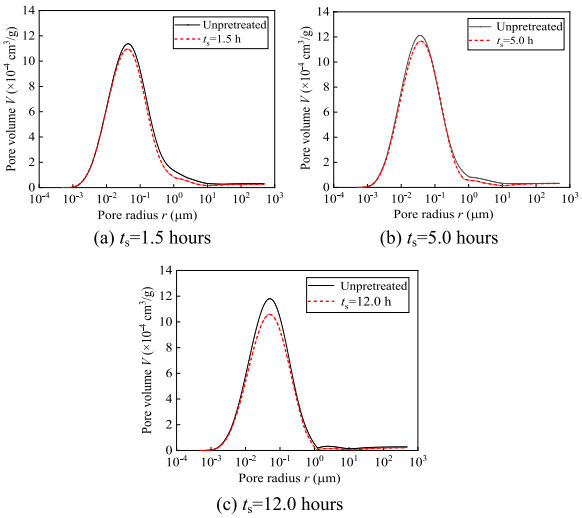

Fig. 5 Pore size distribution curves of PRCAs with different soaking durations in water glass solution

Table 4 Pore size distribution data of PRCAs with different soaking durations

Samples	Gel pores/% (< 10 nm)	Transitional pores/% (10 nm–100 nm)	Capillary pores /% (100 nm–1000 nm)	Macropores /% (> 1000 nm)	Most probable pore radius /nm
RCA1	11.60	56.43	24.87	7.10	43.76
RCA2	13.98	57.87	21.62	6.54	35.53
RCA3	10.52	57.99	27.67	3.82	50.27
PRCA1-1.5	12.62	58.93	23.27	5.18	40.82
PRCA2-5.0	14.19	59.88	21.28	4.66	38.08
PRCA3-12.0	10.92	58.58	28.00	2.50	50.27

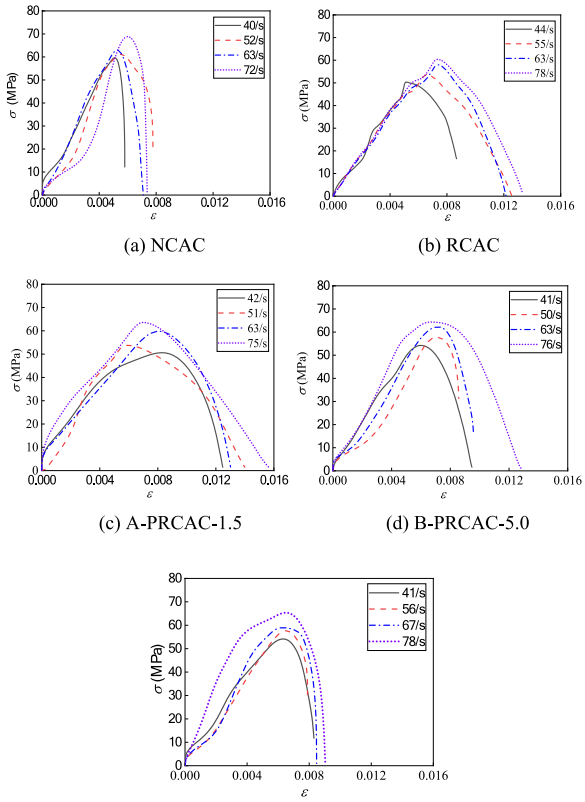

(a) NCAC (b) RCAC

(c) A-PRCAC-1.5 (d) B-PRCAC-5.0

(e) C-PRCAC-12.0

Fig. 6 Dynamic compressive stress–strain curves of concrete specimens with different ρ_{prca}

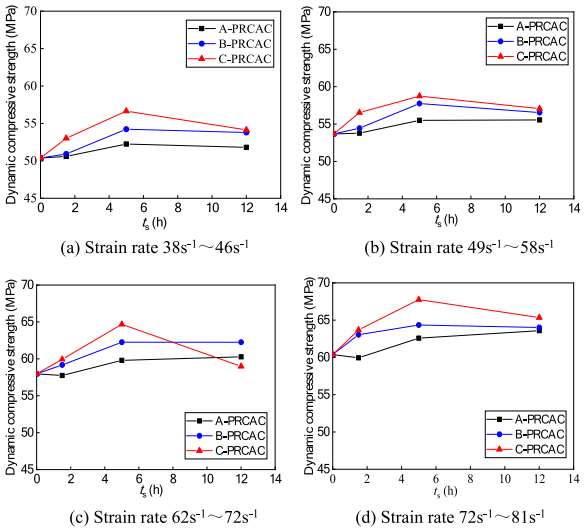

(a) Strain rate 38s^{-1}～46s^{-1} (b) Strain rate 49s^{-1}～58s^{-1}

(c) Strain rate 62s^{-1}～72s^{-1} (d) Strain rate 72s^{-1}～81s^{-1}

Fig. 7 Variation in the dynamic compressive strength of PRCAC with the soaking time t_s

4 Influence of ρ_{prca} on Dynamic Compressive Performance of Concrete

4.1 Dynamic Compressive Stress–Strain Curve

The raw waveform data were first filtered to remove clutter signals, and the extracted incident, reflected, and transmitted wave signals were then substituted into Eqs. (1) and (2) to derive the stress–strain curve. The average strain rate under each condition was calculated by dividing the peak strain at peak stress by the loading duration. Fig. 6 displays the dynamic compressive stress–strain curves of the NCAC, RCAC, A-PRCAC-1.5, B-PRCAC-5.0, and C-PRCAC-12.0 specimens under different strain rates (40–78/s).

Fig. 6 shows that the stress–strain curve of NCAC exhibits a steep decline, indicating brittle behavior of the concrete. In contrast, the curves of RCAC and PRCAC show a relatively gradual decline, demonstrating improved ductility. Overall, as the strain rate increases, the peak stress exhibits an increasing trend. Compared to PRCAC with PRCA incorporation ratios (ρ_{prca}) of 35% and 70%, the descending segment of the stress–strain curve for PRCAC with ρ_{prca} of 100% became steeper, suggesting increased brittleness of the concrete. This behavior is primarily attributed to the reduction of internal microcracks in the pretreated aggregates. As the incorporation ratio of PRCAs increased, fewer cracks developed in the concrete under impact loading. However, the concrete specimens still rapidly lost their load-bearing capacity, possibly because the PRCAs absorbed energy and fractured, leading to a sudden stress drop.

4.2 Dynamic Compressive Strength

To further investigate the effects of PRCA incorporation ratio and pretreatment duration on the dynamic mechanical properties of concrete, we analyzed the variation in the dynamic compressive strength of PRCAC with the soaking time (t_s) of water glass solution at different strain rates, as shown in Fig. 7. The compressive strength at $t_s = 0$ h corresponds to the control group (RCAC).

The dynamic compressive strength of PRCAC is sensitive to strain rate. Within the strain rate range of 40 s^{-1} ~ 79 s^{-1}, the dynamic compressive strength of concrete increases gradually with strain rate, showing an average enhancement of 19.3%. Under dynamic compression, PRCA improves the impact resistance of concrete, primarily because the water glass solution modifies the old mortar area, enhancing its compactness. Additionally, a reduction in C–H content within the old mortar enhances the performance of the interfacial transition zone (ITZ) between RCA and the old mortar (Qiu et al., 2024). As ρ_{prca} increases, the dynamic compressive strength of PRCAC increases. When ρ_{prca} was 35%, the maximum average increase in dynamic compressive strength under three types of t_s was only 3.8% compared to RCAC at similar strain rate levels. This indicated that the improvement in dynamic compressive strength was relatively limited at low ρ_{prca}. However, when ρ_{prca} reached 100%, the maximum average increase under the same conditions rose to 11.4% compared to RCAC. Fig. 7 also shows that for the same ρ_{prca}, the dynamic compressive strength of concrete initially increased and then decreased with increasing t_s, reaching its maximum at a t_s of 5.0 h. For instance, in B-PRCAC under similar strain rate conditions, the average dynamic compressive strength increased by 1.4%, 7.3%, and 4.9% at t_s values of 1.5 h, 5.0 h, and 12.0 h, respectively. The optimal pretreatment effect occurred at a t_s of 5.0 h.

4.3 Strain Rate Effect of Dynamic Increase Factor (DIF)

The dynamic increase factor (DIF) is defined as the ratio of the dynamic compressive strength to the static compressive strength, representing the increase in material strength under dynamic loading (Xiong et al., 2025). Fig. 8 shows the relationship between DIF and the logarithm of strain rate ($\lg \dot{\varepsilon}$) for PRCAC with different t_s. The DIF increases with strain rate, exhibiting an approximately linear relationship with the logarithm of strain rate, which indicates that concrete has a higher DIF at high strain rates. This is because, under high strain rates, the shorter impact time does not allow sufficient time for more energy-absorbing cracks to develop. As a result, the aggregates absorb the excess energy through crushing, which increases the concrete strength and DIF.

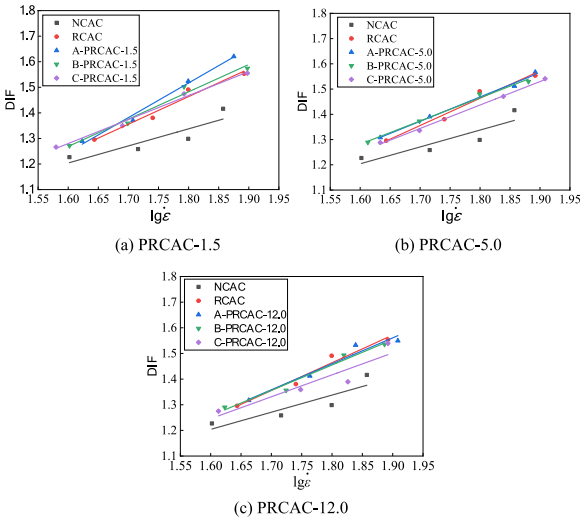

(a) PRCAC-1.5 (b) PRCAC-5.0

(c) PRCAC-12.0

Fig. 8 Changes in DIF with the logarithm of strain rate of PRCAC with different t_s

In addition, as ρ_{prca} increased from 0 to 100%, the average DIF of PRCAC-1.5, PRCAC-5.0, and PRCAC-12.0 decreased by 2.2%, 1.4%, and 1.4%, respectively. This indicates that as a higher ρ_{prca} enhanced the dynamic compressive performance of PRCAC, it simultaneously reduced the strain rate sensitivity of the DIF. This phenomenon is mainly related to the microstructure and failure mechanism of concrete. Higher-strength concrete has lower porosity, a denser cement matrix, and a stronger interfacial transition zone (ITZ). This dense structure requires higher energy for crack propagation, making it more difficult for microcracks to initiate and propagate during dynamic loading. In contrast, low-strength concrete contains more pores, which facilitates the rapid propagation of microcracks under dynamic loads, leading to higher strain rate sensitivity. When the ρ_{prca} was fixed, the slope of the fitted straight lines between DIF and $\lg \dot{\varepsilon}$ decreased first and then increased with the increase of t_s. Notably, samples with a t_s of 5.0 h exhibited the minimum slope, indicating that the DIF shows its lowest sensitivity to strain rate at this specific t_s.

5 Effect of Calcium Leaching on Dynamic Compressive Performance of PRCAC

5.1 Dynamic Compressive Stress–Strain Curve

The stress–strain curves of cylindrical specimens with different leaching durations under impact loading are shown in Fig. 9. Overall, the concrete under all tested conditions exhibited strain rate sensitivity, and the slope of the rising section of the curve increased with the strain rate. The peak strain exhibited slight fluctuations, and no clear pattern was observed. However, as

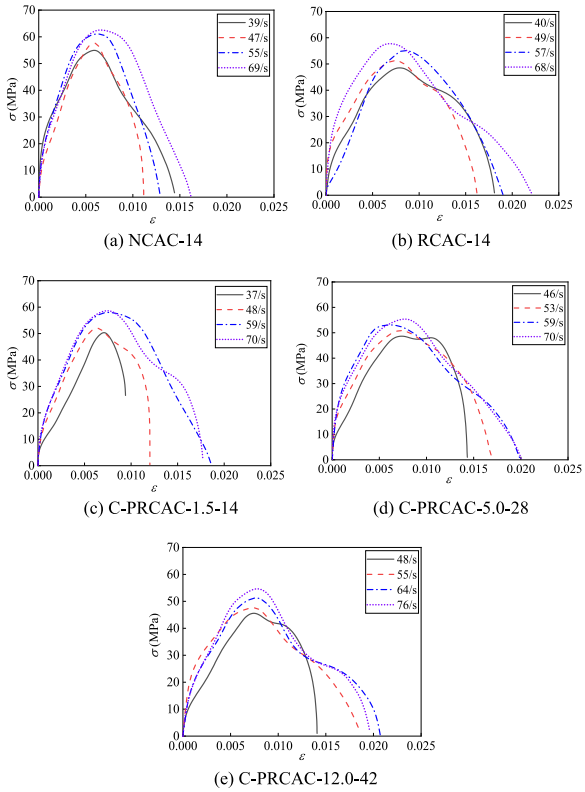

(a) NCAC-14 (b) RCAC-14

(c) C-PRCAC-1.5-14 (d) C-PRCAC-5.0-28

(e) C-PRCAC-12.0-42

Fig. 9 Stress–strain curves of PRCAC with various leaching durations under impact loading

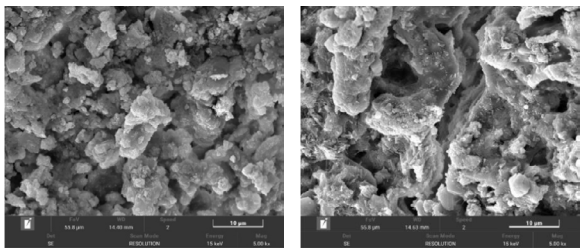

(a) Before calcium leaching (b) After calcium leaching

Fig. 10 SEM images of concrete (5000× magnification)

the leaching duration increased, the slope of the curve's rising section decreased. Before reaching the peak strain, the deformation of the concrete increased gradually, and the descending section of the stress–strain curve became progressively gentler, further improving the concrete's toughness. This was primarily attributed to calcium leaching, which caused decalcification and decomposition of C–H and C–S–H in the concrete, leading to an increase in internal pores (Fig. 10). The peak strain showed an upward trend with increasing leaching duration. When the leaching duration

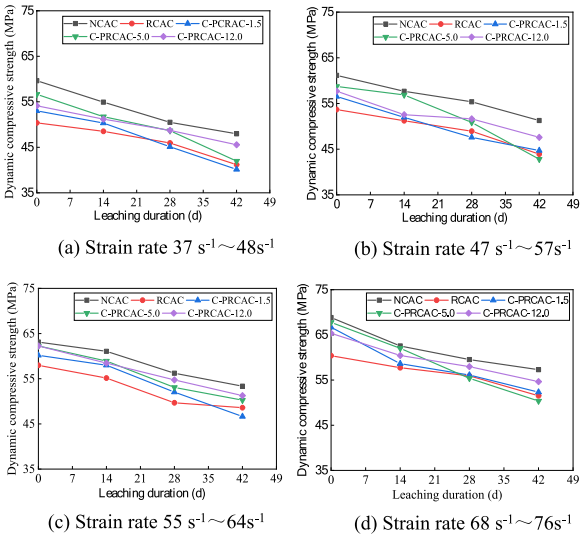

(a) Strain rate 37 s^{-1}～48s^{-1} (b) Strain rate 47 s^{-1}～57s^{-1}

(c) Strain rate 55 s^{-1}～64s^{-1} (d) Strain rate 68 s^{-1}～76s^{-1}

Fig. 11 Changes in dynamic compressive strength of concrete with different leaching duration

increased from 28 to 42 days, the peak strain increased by an average of 14.2%.

5.2 Dynamic Compressive Strength

The variations in dynamic compressive strength of concrete at different strain rates with leaching duration are shown in Fig. 11. It can be seen that the dynamic compressive strength of concrete after leaching remained sensitive to strain rate, and the dynamic compressive strength increased with the increase of strain rate. However, as the leaching duration increased, the dynamic compressive strength of concrete gradually decreased. There were significant differences in the degree of strength degradation among concrete samples with different t_{sth}. Taking C-PRCAC with a leaching duration of 42 days as an example, the average decrease in dynamic compressive strength under three types of t_{sth} was 21.3%, 25.2%, and 15.7%, respectively, compared to non-dissolved concrete. The decrease observed in C-PRCAC-12.0 was smallest. Additionally, the descending section of the C-PRCAC-12.0 curve was the gentlest, exhibiting the smallest slope. When the leaching duration reached 28 days, the dynamic compressive strength of C-PRCAC-12.0 exceeded that of C-PRCAC-5.0 and was second only to that of NCAC. This can be attributed to the higher amount of C–S–H in the aggregate of C-PRCAC-12.0. As the leaching duration increased, the leaching effect developed deeper, and the C–S–H and co-ion effects reduced the leaching of C–H and Ca^{2+}, resulting in better strength retention (Jain & Neithalath, 2009).

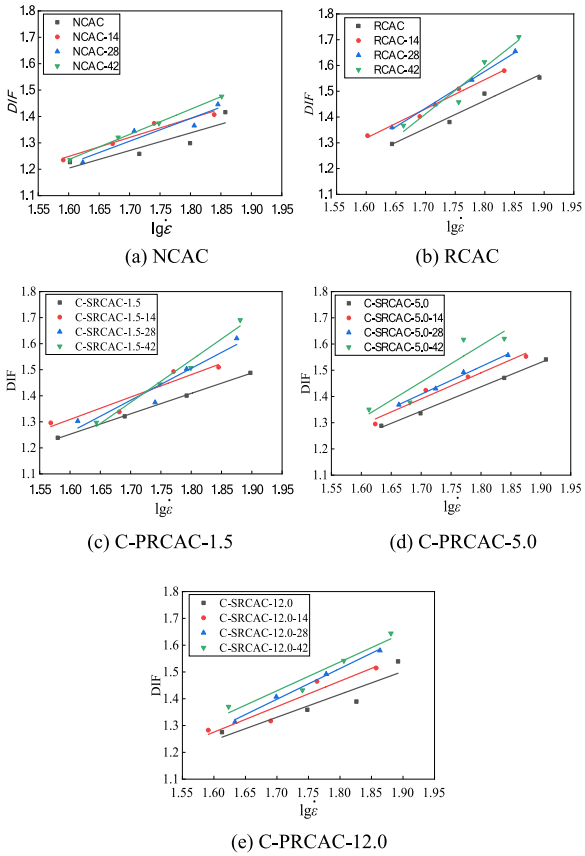

Fig. 12 Changes in DIF with the logarithm of strain rate of concrete with different leaching durations

5.3 Strain Rate Effect of DIF

Fig. 12 shows the variation in DIF with the logarithm of strain rate for concrete with different leaching durations. It can be seen that the DIF had a linearly increasing relationship with the logarithm of strain rate. As the leaching duration increased, the slope of the straight line also gradually increased, indicating that the sensitivity of the increase in dynamic compressive strength to strain rate became greater. The effect of leaching on PRCAC with different t_{sth} varied. Due to its dense internal structure, NCAC experienced relatively small changes in internal pores after leaching. Under impact loading, it can only absorb energy through the crushing of some aggregates. Therefore, although it had the highest dynamic compressive strength, the variation in DIF resulting from changes in strain rate was relatively small. In contrast, RCAC can absorb more energy during impact due to the more pores generated by leaching, resulting in a maximum increase in DIF. As t_{sth} increased, the change in slope generated by the increase in leaching duration gradually decreased, indicating that the strain rate sensitivity of DIF under high leaching duration gradually decreased. This was because, with increasing t_{sth}, the internal pores of the concrete gradually decreased, the leaching resistance gradually increased, and the change in DIF gradually decreased.

6 Constitutive Model of PRCAC Under Dynamic Compression

6.1 Derivation of Constitutive Model

Because concrete is a heterogeneous material with inherent internal defects, its microstructural components are subjected to non-uniform stress distributions under external loading. Li et al. (2020) assumed that the internal damage of concrete was continuous and that the micro-element strength followed a probability distribution. They subsequently proposed a viscoelastic damage constitutive model for concrete, as shown below.

$$\sigma = (1 - D)E_0\varepsilon + \mu\dot{\varepsilon} \tag{4}$$

where E_0 is the initial elastic modulus of concrete, GPa; D is the damage variable; η is the viscosity coefficient.

According to the existing research conclusions in concrete dynamic mechanics, the strength distribution of concrete's internal microstructural elements follows a Weibull probability distribution (Zhou et al., 2024), which can be expressed as follows:

$$D = 1 - \exp\left(-\frac{\varepsilon^m}{\alpha}\right) \tag{5}$$

where m and α are the parameters of the Weibull distribution.

By substituting Eq. (5) into Eq. (4), the theoretical constitutive model of dynamic viscoelastic damage for concrete can be obtained as follows:

$$\sigma = \exp\left(-\frac{\varepsilon^m}{\alpha}\right)E_0\varepsilon + \eta\dot{\varepsilon} \tag{6}$$

To further investigate the effects of the incorporation ratio of PRCAs and leaching duration on the dynamic compressive performance of concrete, we introduce a damage degradation factor ξ, defined as follows:

$$\xi = 1 - \frac{f_{rd,n}}{f_{rd,0}} \tag{7}$$

where $f_{rd,n}$ is the dynamic compressive strength of concrete with the ρ_{prca} of n% or the leaching duration of n, and $f_{rd,0}$ is the dynamic compressive strength of concrete without pretreated aggregates or calcium leaching.

By substituting Eq. (7) into Eq. (6), the theoretical constitutive model of dynamic viscoelastic damage of concrete, which considers the effects of the incorporation

ratio of PRCA and leaching duration, can be expressed as follows:

$$\sigma = (1-\xi)\exp\left(-\frac{\varepsilon^m}{\alpha}\right)E_0\varepsilon + \eta\dot{\varepsilon} \tag{8}$$

The unknown parameters in Eq. (8) can be determined through inversion analysis based on the test results.

6.2 *Model Verification of Dynamic Compressive Test for Concrete with Different ρ_{prca}*

PRCA can improve the compressive strength of concrete. Overall, PRCAC-5.0 exhibited higher dynamic compressive strength before leaching, while PRCAC-12.0 demonstrated better leaching resistance. Therefore, the experimental data for PRCAC-5.0 and PRCAC-12.0 were selected to fit the parameter in the constitutive model of PRCAC with different ρ_{prca}. The values of ξ for concrete at strain rates of 72–81 s^{-1} were calculated, and the ξ-values of PRCAC-5.0 and PRCAC-12.0 with varying PRCA incorporation ratios were statistically analyzed (Fig. 13). The relationships between ξ and ρ_{prca} were fitted using Eqs. (9) and (10).

$$\text{PRCAC - 5.0: } \xi = 10^{-5}\left(-0.569\rho_{\mathrm{prca}}^2 - 60.623\rho_{\mathrm{prca}}\right) - 0.002 \quad R^2 = 0.988 \tag{9}$$

$$\text{PRCAC - 12.0: } \xi = 10^{-5}\left(-0.432\rho_{\mathrm{prca}}^2 - 45.690\rho_{\mathrm{prca}}\right) + 0.003 \quad R^2 = 0.956 \tag{10}$$

It can be seen that the fitting equation well described the relationship between ξ and ρ_{prca} for the two types of PRCAC. According to the actual working conditions, ξ and $\dot{\varepsilon}$ were substituted into Eq. (8) to fit the stress–strain curve of concrete under impact loading. The fitting results of the dynamic constitutive parameters and the fitting stress–strain curves are shown in Fig. 14, respectively. The fitting curve and the experimental curve exhibit a high degree of overlap, indicating that the viscoelastic damage constitutive model effectively characterized the stress–strain relationship of PRCAC with different ρ_{prca}.

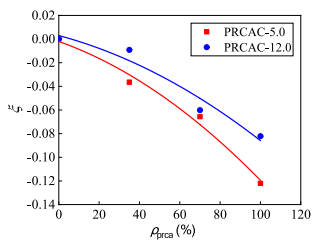

Fig. 13 Changes in damage degradation factor ξ with ρ_{prca}

6.3 Model Verification of Dynamic Compressive Test for Concrete After Calcium Leaching

The stress–strain curves of C-PRCAC-5.0 and C-PRCAC-12.0 under different leaching durations at strain rates of 68 s^{-1} to 76 s^{-1} were selected to fit the parameters in the constitutive model. The statistical analysis of ξ for concrete subjected to different leaching durations is shown in Fig. 15. The fitting equations for the relationship between ξ and leaching duration (t_{le}) are given in Eqs. (11) and (12).

$$\text{C - PRCAC - 5: } \xi = 10^{-5}\left(-1.337t_{\mathrm{le}}^2 + 676t_{\mathrm{le}}\right) - 0.002 \quad R^2 = 0.998 \tag{11}$$

$$\text{C - PRCAC - 12: } \xi = 10^{-5}\left(-3.103t_{\mathrm{le}}^2 + 508t_{\mathrm{le}}\right) + 0.003 \quad R^2 = 0.991 \tag{12}$$

The ξ and $\dot{\varepsilon}$ were substituted into Eq. (8) to fit the stress–strain curves. The fitted results are presented in Fig. 16. The fitting curves are in good agreement with the experimental curves, demonstrating that the viscoelastic damage constitutive model accurately characterizes the stress–strain behavior of C-PRCAC under different leaching durations.

7 Conclusions

1. Water glass pretreatment significantly improve the performances of recycled coarse aggregates (RCAs). It reduces water absorption, crushing index, and porosity in RCAs. Although these indicators for pretreated RCAs (PRCAs) remain inferior to those of natural coarse aggregates (NCAs), the pretreatment narrows the performance gap between RCAs and NCAs, especially for low-quality RCAs.
2. The dynamic compressive strength of pretreated recycled coarse aggregate concrete (PRCAC) increases with the strain rate, demonstrating significant strain-rate sensitivity. Furthermore, the strength enhances with a higher incorporation ratio of PRCAs. The dynamic increase factor (DIF) for the compressive strength of PRCAC also rises with the strain rate; however, its strain-rate sensitivity decreases as the PRCA incorporation ratio increases.
3. The dynamic compressive strength of PRCAC after calcium leaching exhibits strain rate sensitivity, increasing with higher strain rates. However, as the

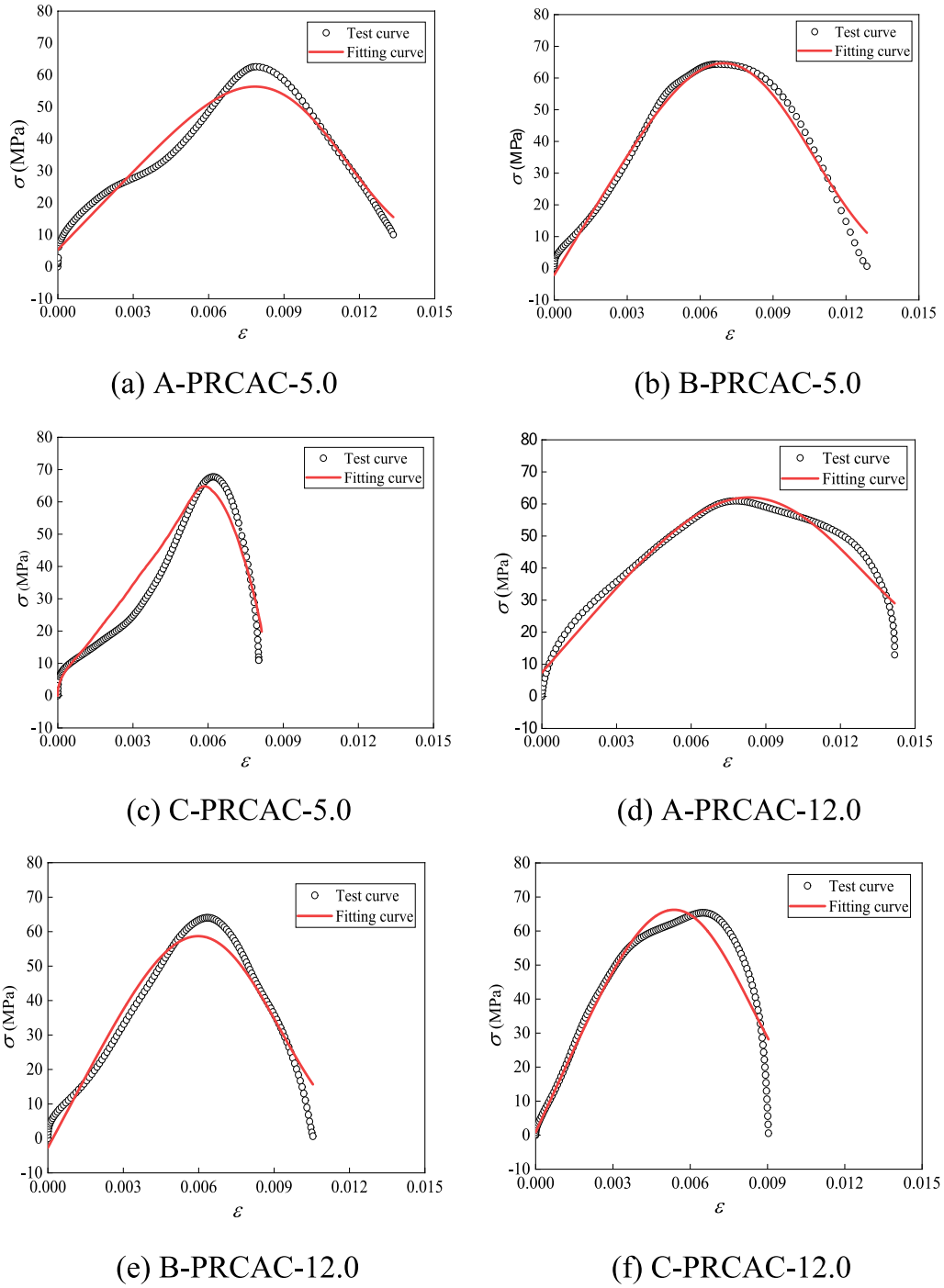

Fig.14 Fitted stress–strain curves of PRCAC with different ρ_{prca}

leaching duration increases, the dynamic compressive strength of PRCAC significantly decreases, while its strain rate sensitivity further increases. Among the three pretreatment durations of RCAs tested in this study, the concrete samples with a 12.0-h pretreatment show the smallest leaching-induced strength reduction. Furthermore, both the DIF of PRCAC and its strain rate sensitivity increase with leaching duration. Clarifying the long-term effects of calcium dissolution on the dynamic performance of RAC could help promote its sustainable application in harsh environments.

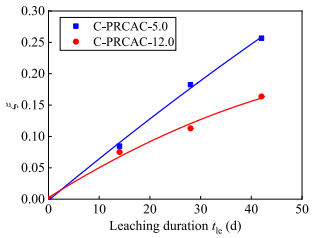

Fig. 15 Changes of damage degradation factor ξ with leaching duration

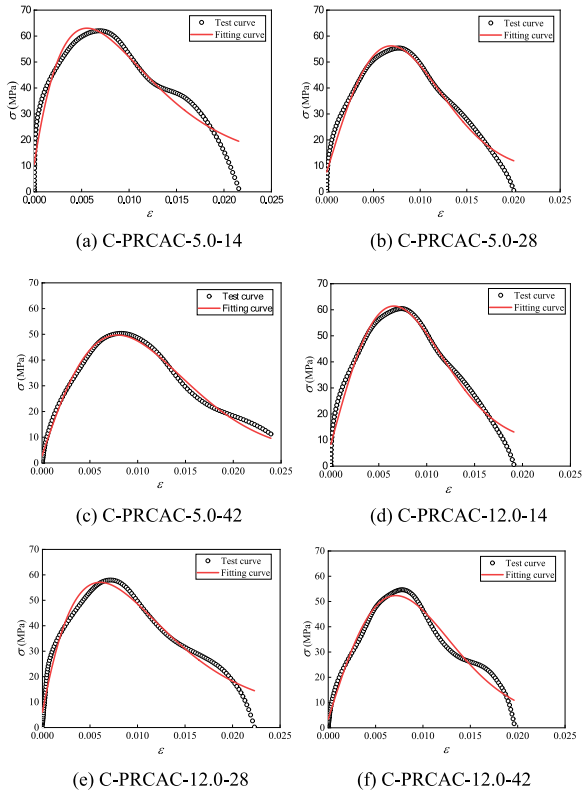

Fig. 16 Fitted stress–strain curves of C-PRCAC under various leaching durations

4. By introducing the damage degradation factor, a theoretical constitutive model of dynamic viscoelastic damage for PRCAC was developed, incorporating the effects of the incorporation ratio of PRCAs and the leaching duration. The model-fitted stress–strain curves show good agreement with the experimental curves.

Acknowledgements
Not applicable.

Author contributions
JJH put forward the research subject and performed the editing of this manuscript. MFL performed the data analysis and writing original draft of this manuscript. CSA performed the data analysis and dynamic mechanical performance tests of concrete. ZW and ZSQ performed the editing of this manuscript. All authors read and approved the final manuscript.

Funding
Financial supports from the National Natural Science Foundation of China (Grant No. 51408192).

Data availability
All data generated or analyzed during this study are included in this published article.

Declarations

Competing interests
The authors declare that they have no competing interests.

Received: 8 January 2025 Accepted: 1 July 2025
Published online: 28 August 2025

References

Allujami, H. M., Abdulkareem, M., Jassam, T. M., Al-Mansob, R. A., Ibrahim, A., Ng, J. L., & Yam, H. C. (2022). Mechanical properties of concrete containing recycle concrete aggregates and multi-walled carbon nanotubes under static and dynamic stresses. *Case Studies in Construction Materials, 17*, Article e01651. https://doi.org/10.1016/j.cscm.2022.e01651

An, S., Jiang, C., Li, S., & Shi, C. (2025). Experimental study on the effect of ion transmission mode on the calcium leaching rate of cementitious materials. *Case Studies in Construction Materials, 22*, Article e04215. https://doi.org/10.1016/j.cscm.2025.e04215

Arjomandi, A., Mousavi, R., Tayebi, M., Nematzadeh, M., Gholampour, A., Aminian, A., & Gencel, O. (2023). The effect of sulfuric acid attack on mechanical properties of steel fiber-reinforced concrete containing waste nylon aggregates: Experiments and RSM-based optimization. *Journal of Building Engineering, 64*, Article 105500. https://doi.org/10.1016/j.jobe.2022.105500

Bao, Z. (2023). Developing circularity of construction waste for a sustainable built environment in emerging economies: New insights from China. *Developments in the Built Environment, 13*, 10010. https://doi.org/10.1016/j.dibe.2022.100107

Bao, Z., Lu, W., Peng, Z., & Ng, S. T. (2023). Balancing economic development and construction waste management in emerging economies: A longitudinal case study of Shenzhen, China guided by the environmental Kuznets curve. *Journal of Cleaner Production, 396*, Article 136547. https://doi.org/10.1016/j.jclepro.2023.136547

Dilbas, H., Cakir, O., & Atis, C. D. (2019). Experimental investigation on properties of recycled aggregate concrete with optimized Ball Milling Method. *Construction and Building Materials, 212*, 716–726. https://doi.org/10.1016/j.conbuildmat.2019.04.007

Ding, Z., Wang, X., & Zou, P. X. W. (2023). Barriers and countermeasures of construction and demolition waste recycling enterprises under circular economy. *Journal of Cleaner Production, 420*, Article 138235. https://doi.org/10.1016/j.jclepro.2023.138235

Duan, H., Miller, T. R., Liu, G., & Tam, V. W. Y. (2019). Construction debris becomes growing concern of growing cities. *Waste Management, 83*, 1–5. https://doi.org/10.1016/j.wasman.2018.10.044

Güneyisi, E., Gesoğlu, M., Algın, Z., & Yazıcı, H. (2014). Effect of surface treatment methods on the properties of self-compacting concrete with recycled aggregates. *Construction and Building Materials, 64*, 172–183. https://doi.org/10.1016/j.conbuildmat.2014.04.090

Guo, J., Cai, J., Chen, Q., Liu, X., Wang, Y., & Zuo, Z. (2019). Dynamic behaviour and energy dissipation of reinforced recycled aggregate concrete beams under impact. *Construction and Building Materials, 214*, 143–157. https://doi.org/10.1016/j.conbuildmat.2019.04.124

Han, N., & Tian, W. (2018). Experimental study on the dynamic mechanical properties of concrete under freeze-thaw cycles. *Structural Concrete, 19*(5), 1353–1362. https://doi.org/10.1002/suco.201700170

Jain, J., & Neithalath, N. (2009). Analysis of calcium leaching behavior of plain and modified cement pastes in pure water. *Cement and Concrete Composites, 31*, 176–185. https://doi.org/10.1016/j.cemconcomp.2009.01.003

Jiang, J., Zhang, W., Zhao, K., Rumongi, B., Zhao, H., & Ma, F. (2024). Study on the calcium dissolution of self-compacting recycled concrete. *Construction and Building Materials, 421*, Article 135723. https://doi.org/10.1016/j.conbuildmat.2024.135723

Jiang, J., Zhao, K., Chen, S., & Lin, M. (2022). Calcium dissolution behaviors of recycled coarse aggregate concrete with the initial stress damage. *Construction and Building Materials, 338*, Article 127620. https://doi.org/10.1016/j.conbuildmat.2022.127620

Khoury, E., Ambrós, W., Cazacliu, B., Sampaio, C. H., & Remond, S. (2018). Heterogeneity of recycled concrete aggregates, an intrinsic variability. *Construction and Building Materials, 175*, 705–713. https://doi.org/10.1016/j.conbuildmat.2018.04.163

Kong, X., Fang, Q., Zhang, J., & Zhang, Y. (2020). Numerical prediction of dynamic tensile failure in concrete by a corrected strain-rate dependent nonlocal material model. *International Journal of Impact Engineering, 137*, Article 103445. https://doi.org/10.1016/j.ijimpeng.2019.103445

Li, S., Yi, X., Liu, M., Lu, J., & Qiu, H. (2023). Non-market valuation of construction waste recycling: Evidence from China. *Journal of Cleaner Production, 412*, Article 137384. https://doi.org/10.1016/j.jclepro.2023.137384

Li, W., Luo, Z., Long, C., Wu, C., Duan, W. H., & Shah, S. P. (2016). Effects of nanoparticle on the dynamic behaviors of recycled aggregate concrete under impact loading. *Materials and Design, 112*, 58–66. https://doi.org/10.1016/j.matdes.2016.09.045

Li, Y., Zhai, Y., Liang, W., Li, Y., Dong, Q., & Meng, F. (2020). Dynamic mechanical properties and visco-elasitc damage constitutive model of freeze-thawed concrete. *Materials, 13*(18), 4056–4074. https://doi.org/10.3390/ma13184056

Liu, Z., Chen, X., Wang, X., & Diao, H. (2022). Investigation on the dynamic compressive behavior of waste tires rubber-modified self-compacting concrete under multiple impacts loading. *Journal of Cleaner Production, 336*, Article 130289. https://doi.org/10.1016/j.jclepro.2021.130289

Lu, C., Yu, Q., Wei, J., Niu, Y., Zhang, Y., Lin, C., Chen, P., Shi, C., & Yang, P. (2024). Influence of interface transition zones (ITZ) and pore structure on the compressive strength of recycled aggregate concrete. *Construction and Building Materials, 456*, Article 139299. https://doi.org/10.1016/j.conbuildmat.2024.139299

Luo, B., Wang, D., & Mohamed, E. (2023). The process of optimizing the interfacial transition zone in ultra-high performance recycled aggregate concrete through immersion in a water glass solution. *Materials Letters, 338*, Article 134056. https://doi.org/10.1016/j.matlet.2023.134056

Petrou, M. F. (2021). A mechanical treatment method for recycled aggregates and its effect on recycled aggregate-based concrete. *Materials*. https://doi.org/10.3390/ma14092186

Qiu, J., Wang, J., Feng, Z., Xiao, Z., & Li, L. (2024). Study on the modification mechanism of recycled brick-concrete aggregate concrete based on water glass solution immersion method. *Journal of Building Engineering, 82*, Article 108303. https://doi.org/10.1016/j.jobe.2023.108303

Rezaei, F., Memarzadeh, A., Davoodi, M. R., Dashab, M. A., & Nematzadeh, M. (2023). Mechanical features and durability of concrete incorporating recycled coarse aggregate and nano-silica: Experimental study, prediction, and optimization. *Journal of Building Engineering, 73*, Article 106715. https://doi.org/10.1016/j.jobe.2023.106715

Selyutina, N., & Smirnov, I. (2023). Dynamic fractures of concrete made of recycled aggregate or reinforced with fibres. *Mechanics of Materials, 179*, Article 104613. https://doi.org/10.1016/j.mechmat.2023.104613

Spaeth, V., & Djerbi Tegguer, A. (2013). Improvement of recycled concrete aggregate properties by polymer treatments. *International Journal of Sustainable Built Environment, 2*(2), 143–152. https://doi.org/10.1016/j.ijsbe.2014.03.003

Tafesse, S., Girma, Y. E., & Dessalegn, E. (2022). Analysis of the socio-economic and environmental impacts of construction waste and management practices. *Heliyon, 8*(3), Article e09169. https://doi.org/10.1016/j.heliyon.2022.e09169

Taghipoor, H., & Sadeghian, A. (2022). Experimental investigation of single and hybrid-fiber reinforced concrete under drop weight test. *Structures, 43*, 1073–1083. https://doi.org/10.1016/j.istruc.2022.07.030

Tan, Y., Sugiyama, T., Hashimoto, K., & Liu, J. (2025). Transport of radioactive elements in concrete due to utilization of recycled aggregate contaminated with nuclides. *Construction and Building Materials, 471*, Article 140689. https://doi.org/10.1016/j.conbuildmat.2025.140689

Tang, Z., Li, W., Tam, V. W. Y., & Luo, Z. (2020). Investigation on dynamic mechanical properties of fly ash/slag-based geopolymeric recycled aggregate concrete. *Composites Part B: Engineering, 185*, Article 107776. https://doi.org/10.1016/j.compositesb.2020.107776

Verian, K. P., Ashraf, W., & Cao, Y. (2018). Properties of recycled concrete aggregate and their influence in new concrete production. *Resources Conservation and Recycling, 133*, 30–49. https://doi.org/10.1016/j.resconrec.2018.02.005

Wang, C., & Xiao, J. (2018). Evaluation of the stress-strain behavior of confined recycled aggregate concrete under monotonic dynamic loadings. *Cement and Concrete Composites, 87*, 149–163. https://doi.org/10.1016/j.cemconcomp.2017.12.012

Wang, H., Lin, J., Chen, L., Shi, J., & He, Y. (2024). Experimental study and model evaluation on BFRP tube-confined RAC cylinders under monotonic axial compression. *Structures, 69*, Article 107307. https://doi.org/10.1016/j.istruc.2024.107307

Wu, H., Liang, C., Zhang, Z., Yao, P., Wang, C., & Ma, Z. (2023). Utilizing heat treatment for making low-quality recycled aggregate into enhanced recycled aggregate, recycled cement and their fully recycled concrete. *Construction and Building Materials, 394*, Article 132126. https://doi.org/10.1016/j.conbuildmat.2023.132126

Wu, T., Jin, L., Yu, H., Qiao, L., Zhao, Y., & Zhou, P. (2025). Mesoscale numerical investigation of chloride transport in recycled aggregate concrete considering calcium leaching: Multi-phase and multi-interface. *Structures, 78*, Article 109307. https://doi.org/10.1016/j.istruc.2025.109307

Wu, Z., Cui, Y., Barrett, A. G., Moreno, M. M., & Deng, Y. (2019). Role of surrounding soils and pore water in calcium carbonate precipitation in railway tunnel drainage system. *Transportation Geotechnics, 21*, Article 100257. https://doi.org/10.1016/j.trgeo.2019.100257

Wyrzykowski, M., McDonald, P., Scrivener, K., & Lura, P. (2017). Water redistribution within the microstructure of cementitious materials due to temperature changes studied with 1H NMR. *Journal of Physical Chemistry C, 121*(50), 27950–27962. https://doi.org/10.1021/acs.jpcc.7b08141

Xing, W., Tam, V. W., Le, K. N., Hao, J. L., & Wang, J. (2023). Life cycle assessment of sustainable concrete with recycled aggregate and supplementary cementitious materials[J]. *Resources, Conservation and Recycling, 193*, Article 106947. https://doi.org/10.1016/j.resconrec.2023.106947

Xiong, Z., Chen, X., Fan, C., Chen, N., & Shi, Z. (2025). High strain rate dynamic behavior of autoclaved aerated concrete: Insights from Split Hopkinson Pressure Bar testing. *Construction and Building Materials, 472*, Article 140968. https://doi.org/10.1016/j.conbuildmat.2025.140968

Xiong, Z., Wei, W., He, S., Liu, F., Luo, H., & Li, L. (2021). Dynamic bond behaviour of fibre-wrapped basalt fibre-reinforced polymer bars embedded in sea sand and recycled aggregate concrete under high-strain rate pull-out tests. *Construction and Building Materials, 276*, Article 122195. https://doi.org/10.1016/j.conbuildmat.2020.122195

Yang, J., Guo, Y., Tam, V. W. Y., Tan, J., Shen, A., Zhang, C., & Zhang, J. (2022). Feasibility of recycled aggregates modified with a compound method involving sodium silicate and silane as permeable concrete aggregates. *Construction and Building Materials, 361*, Article 129747. https://doi.org/10.1016/j.conbuildmat.2022.129747

Yin, J., Kang, A., Xiao, P., Kou, C., Gong, Y., & Xiao, C. (2023). Influences of spraying sodium silicate based solution/slurry on recycled coarse aggregate. *Construction and Building Materials, 377*, Article 130924. https://doi.org/10.1016/j.conbuildmat.2023.130924

Zhang, H., Liu, W., Lin, X., Su, S., & Zhao, B. (2021). To ameliorate the performance of recycled aggregate concrete (RAC) by pre-treating aggregate in sulfoaluminate cement slurry and water glass solution. *Journal of Building Engineering, 44*, Article 103364. https://doi.org/10.1016/j.jobe.2021.103364

Zhang, H., Tang, H., Yang, Z., & Gong, F. (2025). Chloride-induced reinforcement corrosion and rust filling in recycled aggregate concrete. *Construction and Building Materials, 486*, Article 141997. https://doi.org/10.1016/j.conbuildmat.2025.141997

Zhang, H., Zhao, Y., Meng, T., & Shah, S. P. (2015). The modification effects of a nano-silica slurry on microstructure, strength, and strain development of recycled aggregate concrete applied in an enlarged structural test. *Construction and Building Materials, 95*, 721–735. https://doi.org/10.1016/j.conbuildmat.2015.07.089

Zhang, R., Xie, D., Wu, K., & Wang, J. (2023a). Optimization of sodium alginate aided bio-deposition treatment of recycled aggregates and its application in concrete. *Cement and Concrete Composites, 139*, Article 105031. https://doi.org/10.1016/j.cemconcomp.2023.105031

Zhang, W., Shi, D., Shen, Z., Zhang, J., Zhao, S., Gan, L., Li, Q., Chen, Y., & Tang, P. (2023b). Influence of chopped basalt fibers on the fracture performance of concrete subjected to calcium leaching. *Theoretical and Applied Fracture Mechanics, 125*, Article 103934. https://doi.org/10.1016/j.tafmec.2023.103934

Zhao, H., Xiang, Y., Zhang, B., Qin, X., Xu, W., Wang, W., Tian, Q., & Liu, J. (2021). Effects of temperature rising inhibitor and shrinkage reducing admixture on pore structure of early-age cement paste. *Construction and Building Materials, 306*, Article 124896. https://doi.org/10.1016/j.conbuildmat.2021.124896

Zhao, X., Zhou, F., Wang, W., Kong, D., Liu, J., & Wu, H. (2023). Dynamic compressive behavior of polyethylene fiber reinforced high strength and high ductility concrete over wide ranges of strain rate. *Journal of Building Engineering, 80*, Article 107953. https://doi.org/10.1016/j.jobe.2023.107953

Zhou, D., Chen, D., Yang, F., Mei, J., Yao, Y., & Deng, Y. (2024). Freeze-thaw damage analysis and life prediction of modified pervious concrete based on Weibull distribution. *Case Studies in Construction Materials, 20*, Article e03305. https://doi.org/10.1016/j.cscm.2024.e03305

Publisher's Note

Jian-Hua Jiang Associate Professor, College of Civil and Transportation Engineering, Hohai University, Nanjing, China, 210024

Fu-Liang Ma Postgraduate, College of Civil and Transportation Engineering, Hohai University, Nanjing, China, 210024

Si-An Chen Postgraduate, College of Civil and Transportation Engineering, Hohai University, Nanjing, China, 210024

Wei Zhang Postgraduate, College of Civil and Transportation Engineering, Hohai University, Nanjing, China, 210024

Si-Qi Zhao Postgraduate, College of Civil and Transportation Engineering, Hohai University, Nanjing, China, 210024